Modeling of Modified Vehicle Crashworthiness using a Double Compound Pendulum

Gulshan Noorsumar[a], Svitlana Rogovchenko[b], Dmitry Vysochinskiy[c] and Kjell G. Robbersmyr[d]

Department of Engineering Sciences, University of Agder, Grimstad, Norway

Keywords: Double Pendulum, Vehicle Collisions, Torsional Spring, Lumped Parameter Model, Modified Vehicle.

Abstract: Vehicle crash modeling has been a challenge for researchers for several decades. Occupant injury prevention and prediction is a critical area within vehicle safety design. The modeling of material failure in structural members during a full frontal crash has been presented in this paper. This study presents a Lumped Parameter Model (LPM) with an elastic double compound pendulum replicating the impact kinematics. The model defined using Lagrangian formulation; presents a novel methodology to represent material fracture caused due to heat affected zones or welding in Ultra High Strength Steels (UHSS) in a non-linear crash event. The material fracture leads to rotation of the vehicle; presented in the form of torsional springs in the LPM developed in this study. The Simulink model has been validated with a finite element simulation and shows good correlation to predict parameters crucial to design for occupant protection in a vehicle crash.

1 INTRODUCTION

Traffic accidents lead to many fatalities on the roads worldwide. It is one of the major global problems which demands attention. With an increasing global population, transportation demands have increased leading to more cars on roads and appropriate efforts to reduce traffic related injuries should be taken. Automakers and researchers strive to achieve stringent safety regulations improving the safety of occupants and road users in a crash (Noorsumar et al., 2021a). Real-time crash impacts had been the preferred mode of safety testing for new cars for decades; the emergence of mathematical models have reduced physical testing during the development process. There is still a need to further decrease the dependence on physical tests for crashworthiness assessment of vehicles.

Noorsumar et al. (Noorsumar et al., 2021a) have reviewed the mathematical models used in the industry and academia to replicate vehicle impacts. Finite Element Methods (FEM) have found applications in several areas of safety research; one of the early contributions to the theory and applications of FEM in dynamic crush modeling was made in (Pifko and Winter, 1981). The increasing use of FEM in modeling vehicle and occupant models in the automotive industry is reported in (Böttcher et al., 2005).

Lumped Parameter Models (LPM) are often applied in crash modeling due to their low computational requirements and faster results but they produce lower accuracy as compared to FE Models. Kamal presented an LPM for vehicle impact in 1970 (Kamal, 1970). His work paved the way for several studies targeting parameter identification in impact loadcases (Benson et al., 1986), (Mentzer et al., 1992). Elkady et al. have developed models to explore the effects of Vehicle Dynamics Control Systems (VDCS) on the crash mitigation for an impact with a rigid barrier (Elkady et al., 2012),(Elkady and Elmarakbi, 2012). These models use non-linear springs to represent the front-end deformation; the studies show good correlation with the tests. LPMs have been used to represent flexible bodies in different applications where modeling of joints is crucial to replicate the system (Subedi et al., 2020). Occupant modeling for vehicle crashworthiness has been studied by several researchers using LPMs; Ionut et al. present a 2-dimensional model with 2 vehicles and 2 occupants using Lagrangian mechanics (Ionut et al., 2017).

Deceleration of large vehicles along with rotation of the vehicle in different axes is the leading cause of

[a] https://orcid.org/0000-0002-6718-4508
[b] https://orcid.org/0000-0001-8002-4974
[c] https://orcid.org/0000-0002-0453-0012
[d] https://orcid.org/0000-0001-9578-7325

Noorsumar, G., Rogovchenko, S., Vysochinskiy, D. and Robbersmyr, K.
Modeling of Modified Vehicle Crashworthiness using a Double Compound Pendulum.
DOI: 10.5220/0011306100003274
In *Proceedings of the 12th International Conference on Simulation and Modeling Methodologies, Technologies and Applications (SIMULTECH 2022)*, pages 102-111
ISBN: 978-989-758-578-4; ISSN: 2184-2841

head and chest injuries (Chang et al., 2006b). More recently, the Lagrangian formulation in an LPM employing a novel two-phase technique for the complex non-linear impact scenario was suggested (Noorsumar et al., 2021b). The obtained results reinforce the conclusions that occupant's contact with a headliner during the vehicle pitch and drop lead to more serious head and neck injuries ((Chang et al., 2006b), (Chang et al., 2006a)). Good correlation with pitching data from validation tests is demonstrated. There is, however, a need to improve prediction models for better safety for unbelted occupants in crashes. The complexity of the model further increases if we want to incorporate material failure in the LPM. There are several manufacturing and joining processes involved in producing and repairing the parts of the vehicle which may result in reduced crashworthiness. Several papers investigate the weldability and heat treatment of Ultra High Strength Steels (UHSS) and the material changes due to the exposure of the workpiece to thermal changes (Noorsumar et al., 2021c), (Noorsumar et al., 2020), (Zhang et al., 2008). Amirthalingam studied the change in material behavior due to welding and heat treatment of dog-bone samples (Amirthalingam et al., 2009). Capturing these material behaviour changes in an LPM is a difficulty yet to be addressed by researchers in the industry and the academia. This challenge has also posed a limitation to use of LPMs in the automotive industry. Pavlov used an inverted pendulum to represent a vehicle undergoing pitching (Pavlov, 2019). Occupant kinematics using a pendulum was presented in (Cyrén and Johansson, 2018). Double pendulum models have been used to define impact with a rough surface in ((Sypniewska-Kamińska et al., 2017), (Sypniewska-Kamińska et al., 2016)). In this paper, we study the crash impact of a modified vehicle with welds on the UHSS members against a rigid non-deformable barrier. We a compound double pendulum model with polar coordinates to define the system. In our model,the vehicle impacts the barrier at 0% offset at 56 kmph and the body acts like a compound elastic double pendulum in motion.

2 METHODOLOGY

Our model represents a vehicle with welds and a heat affected zone (HAZ) leading to failures in the structural members during a full frontal impact. A double pendulum has been employed to replicate the scenario in the LPM; it includes two mass components representing the compartment before and after the welded zone. The weld is represented by a torsional joint in the model allowing the rotation of the body about the joint by a small angle θ_2. The assumptions in the model include (Noorsumar et al., 2021b):

- A full frontal impact generally leads to rotation about the *y*-axis, hence only vehicle rotations about the *y*-axis (pitching) were considered in the model.
- Energy losses like friction and heat losses were neglected.
- It was assumed that the front-end spring and damper characteristics are piece-wise linear with four breakpoints, even though the system behaves non-linearly in a crash.
- The welds are assumed to fail during the impact due to the behaviour of UHSS members affected by previous welding and heat treatment.
- A dimensionless torsional spring represents the weld and failure of the model occurs along the *y* axis.

The motion of a double pendulum is described as follows: the pendulum swings back and forth about the pivot point as shown in Figure 1. Under impact, the vehicle behaves like a pendulum rotating around the pivot point, that is, an impact point in this case, thus, causing the pitching. As a result of the ground acting as a constraint, the vehicle cannot sway back and forth. The deformable front end crumple zone is represented with a spring and damper system for the pendulum; the suspensions acting as a constraint to prevent the pendulum to rotate beyond a certain angle. The 3 Degrees of Freedom (DOF) LPM is defined to determine the governing equations of motion; the system is simplified by converting the cartesian coordinates to polar coordinates.

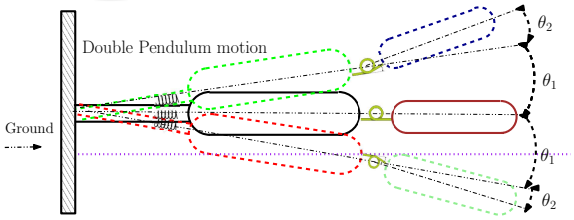

Figure 1: Vehicle body rotating like a pendulum about the impact point.

Figure 2 shows the model of the vehicle impacting a rigid barrier. The front end deformation is represented by the elastic pendulum; the spring and damper coefficients are defined using a piecewise linear function with five breakpoints. The torsional spring connects the mass components before and after the welded zone.The LPM containing two mass

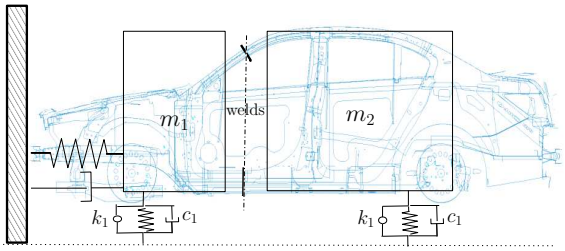

Figure 2: Vehicle body with welds and the occupant compartments divided into lumped mass systems.

components along with the constraints is presented in Figure 3

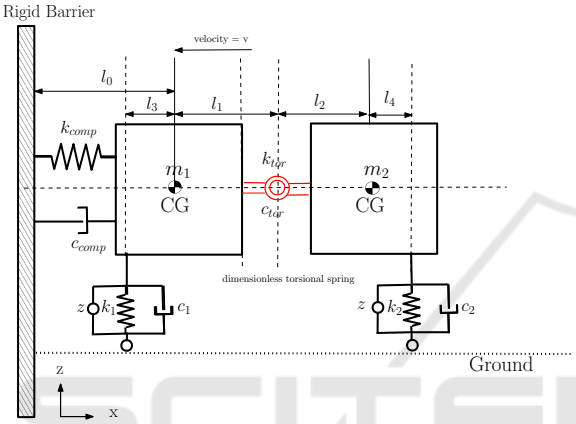

Figure 3: LPM of the vehicle impacting the rigid barrier at time $t = 0$.

The event has been divided into three phases:

- Deformation of the front end leading to energy absorption modeled as an elastic spring.
- Rotation of the vehicle body about the impact point with an angle θ_1.
- Failure of the welds leading to rotation of the vehicle about the torsional joint with an angle θ_2.

The double pendulum model replicating the vehicle rotating about the torsional spring with an angle θ_2 is shown in Figure 4.

2.1 Parameter Identification for Front End Spring and Damper Characteristics

The front end spring damper characteristics were defined using an algorithm developed by the authors (Noorsumar et al., 2021b). The gradient descent optimization algorithm has been modified to fit the force-deformation curve for the entire dynamic event.

The spring and damper coefficients derived from the algorithm are presented in the next section. The

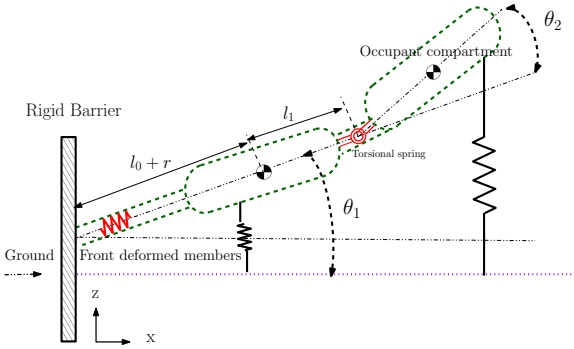

Figure 4: Vehicle body rotating about the impact point after front-end deformation.

non-linear force deformation curve have been approximated to represent the front end system in the LPM. The stiffness k and spring force F_k are related by the equation (1). Similarly, the damper coefficient c is related to the damping force F_c by the equation (2) ((Elkady and Elmarakbi, 2012), (Noorsumar et al., 2021b)).

$$F_k = k(x) \cdot x, \tag{1}$$

$$F_c = c(\dot{x}) \cdot \dot{x}, \tag{2}$$

where

$$k(x) = \begin{cases} \frac{(k_2-k_1)\cdot|\hat{x}|}{x_1} + k_1, & \text{for } |\hat{x}| \le x_1, \\ \frac{(k_3-k_2)\cdot(|\hat{x}|-x_1)}{(x_2-x_1)} + k_2, & \text{for } x_1 \le |\hat{x}| \le x_2, \\ \frac{(k_4-k_3)\cdot(|\hat{x}|-x_2)}{(x_3-x_2)} + k_3, & \text{for } x_2 \le |\hat{x}| \le x_3, \\ \frac{(k_5-k_4)\cdot(|\hat{x}|-x_3)}{(x_4-x_3)} + k_4, & \text{for } x_3 \le |\hat{x}| \le x_4, \\ \frac{(k_6-k_5)\cdot(|\hat{x}|-x_4)}{(x_5-x_4)} + k_5, & \text{for } x_4 \le |\hat{x}| \le x_5, \\ \frac{(k_7-k_6)\cdot(|\hat{x}|-x_5)}{(C-x_5)} + k_6, & \text{for } x_5 \le |\hat{x}| \le C. \end{cases}$$

The damper characteristics are defined similar to the spring characteristics in the model:

$$c(\dot{x}) = \begin{cases} \frac{(c_2-c_1)\cdot|\dot{\hat{x}}|}{\dot{x}_1} + c_1, & \text{for } |\dot{\hat{x}}| \le \dot{x}_1, \\ \frac{(c_3-c_2)\cdot(|\dot{\hat{x}}|-\dot{x}_1)}{(\dot{x}_2-\dot{x}_1)} + c_2, & \text{for } \dot{x}_1 \le |\dot{\hat{x}}| \le \dot{x}_2, \\ \frac{(c_4-c_3)\cdot(|\dot{\hat{x}}|-\dot{x}_2)}{(\dot{x}_3-\dot{x}_2)} + c_3, & \text{for } \dot{x}_2 \le |\dot{\hat{x}}| \le \dot{x}_3, \\ \frac{(c_5-c_4)\cdot(|\dot{\hat{x}}|-\dot{x}_3)}{(\dot{x}_4-\dot{x}_3)} + c_4, & \text{for } \dot{x}_3 \le |\dot{\hat{x}}| \le \dot{x}_4, \\ \frac{(c_6-c_5)\cdot(|\dot{\hat{x}}|-\dot{x}_4)}{(\dot{x}_5-\dot{x}_4)} + c_5, & \text{for } \dot{x}_4 \le |\dot{\hat{x}}| \le \dot{x}_5, \\ \frac{(c_7-c_6)\cdot(|\dot{\hat{x}}|-\dot{x}_5)}{(v_0-\dot{x}_5)} + c_6, & \text{for } \dot{x}_5 \le |\dot{\hat{x}}| \le v_0, \end{cases}$$

where k is the front end spring coefficient, c is the front end damper coefficient, $\hat{x}$ is the computed vehicle deformation, $\dot{x}$ is the vehicle velocity, $\dot{\hat{x}}$ is the computed vehicle velocity, C is the maximum dynamic crush, v_0 is the velocity at the time of maximum dynamic crush. The optimization algorithm which minimizes the error between the test and computed values has been used to determine the acceleration, velocity and deformation of the vehicle (Noorsumar et al., 2021b).

2.2 Defining the Equations of Motion

The governing equations of motion have been modeled using the relativistic Lagrangian formulation (Goldstein et al., 2002).

$$\frac{d}{dt}\frac{\partial L}{\partial \dot{q}_i} - \frac{\partial L}{\partial q_i} + \frac{\partial D}{\partial q_i} = Q_i, \tag{3}$$

where, in general case, $L = T - V$, T is the total kinetic energy of the system equal to the sum of the kinetic energies of the particles, $q_i, i = 1,...,n$ are generalized coordinates and V is the potential energy of the system. Here D is the dissipation function and Q_i is the external force acting on the system; in this case it is the vertical component of the force experienced by the vehicle at the time of maximum dynamic crush (Noorsumar et al., 2021a).

The cartesian system is converted to polar coordinates; the horizontal and vertical coordinates for the two mass system (x_1,y_1) and (x_2,y_2) and the rotations (θ_1 and θ_2) about the y-axis have been represented in (4)-(7):

$$x_1 = [l_0 + r(t)]\cos\theta_1(t), \tag{4}$$

$$z_1 = [l_0 + r(t)]\sin\theta_1(t), \tag{5}$$

$$x_2 = [l_0 + r(t)]\cos\theta_1(t) + l_1\cos\theta_1(t) + l_2\cos\theta_2(t), \tag{6}$$

$$z_2 = [l_0 + r(t)]\sin\theta_1(t) + l_1\sin\theta_1(t) + l_2\sin\theta_2(t), \tag{7}$$

where l_0 is the distance from the center of gravity (CG) of mass m_1 to the point of impact of the vehicle in the rest position, l_1 is the distance from the CG_{m1} to the front suspension, l_2 is the distance from the CG_{m2} to the rear suspension, $r(t)$ is the displacement along the polar radius of the elastic pendulum spring, t is the time, and r, θ_1 and θ_2 are the radius and angles in polar coordinates respectively. Taking the derivatives with respect to time of x_1, x_2 and z_1, z_2 we obtain (8)-(11):

$$\dot{x_1} = \dot{r}\cos\theta_1 - (l_0 + r)\sin\theta_1 \cdot \dot{\theta_1}, \tag{8}$$

$$\dot{z_1} = \dot{r}\sin\theta_1 + (l_0 + r)\cos\theta_1 \cdot \dot{\theta_1}, \tag{9}$$

$$\dot{x_2} = \dot{r}\cos\theta_1 - (l_0 + r)\sin\theta_1 \cdot \dot{\theta_1} - l_1\dot{\theta_1}\sin\theta_1 - l_2\dot{\theta_2}\sin\theta_2, \tag{10}$$

$$\dot{z_2} = \dot{r}\sin\theta_1 + (l_0 + r)\cos\theta_1 \cdot \dot{\theta_1} - l_1\dot{\theta_1}\sin\theta_1 - l_2\dot{\theta_2}\sin\theta_2, \tag{11}$$

where $\dot{x_1}$, $\dot{x_2}$, $\dot{z_1}$ and $\dot{z_2}$ represent the velocity of the mass components in horizontal and vertical directions. Squaring both sides of the equations gives

$$\dot{x_1}^2 = \dot{r}^2\cos^2\theta_1 + (l_0 + r)^2\sin^2\theta_1 \cdot \dot{\theta_1}^2 - 2\dot{r}\cos\theta_1 \cdot (l_0 + r)\sin\theta_1 \cdot \dot{\theta_1}, \tag{12}$$

$$\dot{z_1}^2 = \dot{r}^2\sin^2\theta_1 + (l_0 + r)^2\cos^2\theta_1 \cdot \dot{\theta_1}^2 + 2\dot{r}\cos\theta_1 \cdot (l_0 + r)\sin\theta_1 \cdot \dot{\theta_1}, \tag{13}$$

$$\dot{x_2}^2 = \dot{x_1}^2 + l_1^2\dot{\theta_1}^2\sin\theta_1^2 + l_2^2\dot{\theta_2}^2\sin\theta_2^2 - 2\dot{x_1}l_1\dot{\theta_1}\sin\theta_1 + 2l_1l_2\dot{\theta_1}\dot{\theta_2}\sin\theta_1\sin\theta_2 - 2\dot{x_1}l_2\dot{\theta_2}\sin\theta_2, \tag{14}$$

$$\dot{z_2}^2 = \dot{z_1}^2 + l_1^2\dot{\theta_1}^2\cos^2\theta_1 + l_2^2\dot{\theta_2}^2\cos^2\theta_2 + 2l_1l_2\dot{\theta_1}\dot{\theta_2}\cos\theta_1\cos\theta_2 + 2\dot{z_1}l_1\dot{\theta_1}\cos\theta_1 + 2\dot{z_2}l_2\dot{\theta_2}\cos\theta_2. \tag{15}$$

Adding the terms we have:

$$\dot{x_1}^2 + \dot{z_1}^2 = \dot{r}^2(\cos^2\theta_1 + \sin^2\theta_1) + (l_0 + r)^2 \cdot \dot{\theta_1}^2(\cos^2\theta_1 + \sin^2\theta_1), \tag{16}$$

$$\dot{x_2}^2 + \dot{z_2}^2 = x_1^2 + x_2^2 + l_1^2\dot{\theta_1}^2 + l_2^2\dot{\theta_2}^2 - 2\dot{x_1}l_1\dot{\theta_1}\sin\theta_1 + 2l_1l_2\dot{\theta_1}\dot{\theta_2}\sin\theta_1\sin\theta_2 - 2\dot{x_1}l_2\dot{\theta_2}\sin\theta_2 + 2\dot{z_1}l_1\dot{\theta_1}\cos\theta_1 + 2l_1l_2\dot{\theta_1}\dot{\theta_2}\cos\theta_1\cos\theta_2 + 2\dot{z_1}l_1\dot{\theta_1}\cos\theta_1 + 2\dot{z_1}l_2\dot{\theta_2}\cos\theta_2. \tag{17}$$

The kinetic energy of the system is given by

$$T = \frac{1}{2}[m_1(\dot{x_1}^2 + \dot{z_1}^2) + m_2(\dot{x_2}^2 + \dot{z_2}^2)], \tag{18}$$

or, in polar coordinates,

$$\begin{aligned} T =& \frac{1}{2}m_1[\dot{r}^2 + (l_0+r)^2\dot{\theta_1}^2] \\ &+ \frac{1}{2}m_2[[\dot{r}^2 + (l_0+r)^2\cdot\dot{\theta_1}^2 + l_1^2\cdot\dot{\theta_1}^2 + l_2^2\cdot\dot{\theta_1}^2] \\ &+ 2l_1l_2\dot{\theta_1}\dot{\theta_2}\sin\theta_1\sin\theta_2 \\ &- 2[\dot{r}\cos\theta_1 - (l_0+r)\dot{\theta_1}\sin\theta_1]l_1\dot{\theta_1}\sin\theta_1] \\ &- 2[\dot{r}\cos\theta_1 - (l_0+r)\dot{\theta_1}\sin\theta_1]l_2\dot{\theta_2}\sin\theta_2]. \end{aligned} \tag{19}$$

The potential energy of the system can be found as

$$\begin{aligned} V =& m_1g(l_0+r)\sin\theta_1 \\ &+ m_2g[(l_0+r)\sin\theta_1 + l_1\sin\theta_1 + l_2\sin\theta_2] \\ &+ \frac{1}{2}k_{comp}r_1^2 + \frac{1}{2}k_{tor}\theta_2^2 + \frac{1}{2}k_1r^2 + \frac{1}{2}k_2r_2^2 \end{aligned} \tag{20}$$

where r_1 and r_2 are expressed in terms of r, θ_1, θ_2, l_1, l_2, l_3 as follows:

$$r_1 = (l_0+r-l_3)\theta_1, \tag{21}$$

$$r_2 = (l_0+r+l_1)\theta_1 + l_2\theta_2. \tag{22}$$

Here m_1 is the mass of the lumped body before the weld and HAZ, m_2 is the mass of the occupant compartment after the weld and HAZ, l_3 is the distance from the CG_{m1} to the front suspension, l_2 is the distance from the weld to the CG_{m2}. Simplifying the expression for potential energy in equation (20), we obtain:

$$\begin{aligned} V =& m_1g(l_0+r)\sin\theta_1 + m_2g[(l_0+r)\sin\theta_1 + l_1\sin\theta_1 + l_2\sin\theta_2] \\ &+ \frac{1}{2}k_1(l_0+r-l_3)^2\theta^2 + \frac{1}{2}k_2((l_0+r+l_1)\theta_1 + l_2\theta_2)^2 \\ &+ \frac{1}{2}k_{comp}r_1^2 + \frac{1}{2}k_{tor}\theta_2^2. \end{aligned} \tag{23}$$

Here k_1 and k_2 are the suspension spring coefficients for the front and rear suspensions respectively. Using equations (19) and (23) and Lagrangian formulation, $L = T - V$, we conclude that

$$\begin{aligned} L =& \frac{1}{2}m_1[\dot{r}^2 + (l_0+r)^2\dot{\theta_1}^2] + \frac{1}{2}m_2[\dot{r}^2 + (l_0+r)^2\dot{\theta_2}^2 \\ &+ l_1\dot{\theta_1}^2 + l_2\dot{\theta_2}^2 - 2\dot{r}\dot{\theta_1}l_1\theta_1 \\ &+ 2(l_0+r)l_1\dot{\theta_1}^2\theta_1^2 + 2l_1l_2\dot{\theta_1}\dot{\theta_2}\theta_1\theta_2 \\ &- 2\dot{r}\dot{\theta_2}l_2\theta_2 + 2l_2(l_0+r)\dot{\theta_1}\dot{\theta_2}\theta_1\theta_2] \\ &- m_1g(l_0+r)\sin\theta_1 \\ &- m_2g[(l_0+r)\sin\theta_1 + l_1\sin\theta_1 + l_2\sin\theta_2] \\ &- \frac{1}{2}k_{comp}r_1^2 - \frac{1}{2}k_{tor}\theta_2^2 - \frac{1}{2}k_1r^2 - \frac{1}{2}k_2r_2^2, \end{aligned} \tag{24}$$

The governing equations of motion are:

$$\begin{aligned} Q_r^{ext} =& m_1\ddot{r} + m_2\ddot{r} - m_2l_1(\ddot{\theta_1}\theta_1 + 2\dot{\theta_1}) \\ &- m_2l_2(\ddot{\theta_2}\theta_2 + 2\dot{\theta_2}) - m_1(l_0+r)\dot{\theta_1}^2 \\ &+ m_2(l_0+r)\dot{\theta_1}^2 + m_2l_1\dot{\theta_1}^2\theta_1^2 + m_2l_2\dot{\theta_1}\dot{\theta_2}\theta_1\theta_2 \\ &+ m_1g\theta_1 + m_2g\theta_2 + k_{01}(l_0+r-l_3)\theta_1^2 \\ &+ k_{02}[(l_0+r+l_1)\theta_1^2 + l_2\theta_1\theta_2] + k_{comp}r, \end{aligned} \tag{25}$$

$$\begin{aligned} Q_{\theta_1}^{ext} =& m_1(l_0+r)^2\ddot{\theta_1} + 2m_1(l_0+r)\dot{r}\dot{\theta_1} \\ &+ 2m_2(l_0+r)\dot{r}\dot{\theta_1} + m_2l_1^2\ddot{\theta_1} - m_2l_1\dot{\theta_1}\dot{r} \\ &- m_2l_1\ddot{\theta_1}\dot{r} + 2m_2l_1[\dot{r}\dot{\theta_1}\theta_1^2 + (l_0+r)\theta_1^2\ddot{\theta_1}] \\ &+ 2(l_0+r)l_1\dot{\theta_1}^2\theta_1 + m_2l_1l_2[\ddot{\theta_2}\ddot{\theta_1}\theta_2 + \dot{\theta_2}\dot{\theta_1}\theta_2] \\ &+ m_2l_2[\dot{r}\dot{\theta_2}\theta_1\theta_2 + (l_0+r)\ddot{\theta_2}\theta_1\theta_2 \\ &+ (l_0+r)\dot{\theta_2}\dot{\theta_1}\theta_2] + m_2\dot{r}\dot{\theta_1}l_1 - 2m_2(l_0+r)l_2\dot{\theta_1}^2\theta_1 \\ &- m_2l_1l_2\ddot{\theta_2}\theta_1\theta_2 + m_2l_2(l_0+r)\ddot{\theta_2}\theta_1\theta_2 \\ &+ m_1g(l_0+r) + m_2g[(l_0+r)+l_1] \\ &- k_{01}[l_0+r-l_3]^2\theta_1 - k_{02}[l_0+r+l_1]^2\theta_1 \\ &- k_{02}[l_0+r+l_1]l_2\theta_2, \end{aligned} \tag{26}$$

$$\begin{aligned} Q_{\theta_2}^{ext} =& m_2l_2^2\ddot{\theta_2} + m_2l_1l_2[\ddot{\theta_1}\theta_1\theta_2 + \dot{\theta_1}^2\theta_2 + \dot{\theta_1}\theta_1\dot{\theta_2}] \\ &- m_2l_2[\dot{r}\dot{\theta_1}\theta_1\theta_2 + (l_0+r)\ddot{\theta_1}\theta_1\theta_2 + (l_0+r)\dot{\theta_1}^2\theta_2] \\ &- m_2l_1l_2\dot{\theta_1}\dot{\theta_2}\theta_1 + m_2\dot{r}\dot{\theta_2}l_2 - m_2l_2(l_0+r)\dot{\theta_1}\dot{\theta_2}\theta_1 \\ &+ m_2gl_2 + k_{02}[(l_0+r+l_1)l_2\theta_1 + l_2^2\theta_2] \\ &+ k_r\theta_2 \end{aligned} \tag{27}$$

where Q_r^{ext}, $Q_{\theta_2}^{ext}$ and $Q_{\theta_2}^{ext}$ are the external forces acting on the vehicle. The non-conservative forces in the system are included in the Lagrange's equation of motion in the form of generalized forces expressed with the formulation of virtual work δU (Cyrén and Johansson, 2018):

$$\delta U = \sum_{j=1}^{m} F_j \cdot \delta r_j \tag{28}$$

where F_j are the force components, δr_j are the virtual displacements given by

$$\delta r_j = \sum_{i=1}^{N} \frac{\partial r_j}{\partial q_i}\delta q_i \tag{29}$$

for $j = 1, 2, 3, \ldots, m$. This yields the following equation for virtual work:

$$\begin{aligned} \delta U = F_1 \cdot \sum_{i=1}^{N} \frac{\partial r_j}{\partial q_i}\delta q_i + F_2 \cdot \sum_{i=1}^{N} \frac{\partial r_j}{\partial q_i}\delta q_i + \cdots \\ + F_m \cdot \sum_{i=1}^{N} \frac{\partial r_j}{\partial q_i}\delta q_i. \end{aligned} \tag{30}$$

Using equation (30), we compute the generalized

forces acting the system:

$$\begin{aligned}\delta U = F_{x_1}\cdot\left(\frac{\partial x}{\partial r}\cdot\delta r+\frac{\partial x}{\partial \theta_1}\cdot\delta\theta_1+\frac{\partial x}{\partial \theta_2}\cdot\delta\theta_2\right)\\ +F_{x_2}\cdot\left(\frac{\partial x}{\partial r}\cdot\delta r+\frac{\partial x}{\partial \theta_1}\cdot\delta\theta_1+\frac{\partial x}{\partial \theta_2}\cdot\delta\theta_2\right)\\ +F_{z_1}\cdot\left(\frac{\partial z}{\partial r}\cdot\delta r+\frac{\partial z}{\partial \theta_1}\cdot\delta\theta_1+\frac{\partial z}{\partial \theta_2}\cdot\delta\theta_2\right)\\ +F_{z_2}\cdot\left(\frac{\partial z}{\partial r}\cdot\delta r+\frac{\partial z}{\partial \theta_1}\cdot\delta\theta_1+\frac{\partial z}{\partial \theta_2}\cdot\delta\theta_2\right).\end{aligned} \tag{31}$$

Substituting equations (4) and (5) in equation (31), we get

$$\begin{aligned}dU = F_{x_1}\cdot[(\cos(\theta_1)\delta r-(l_0+r)\sin\theta_1\delta\theta_1]\\ +F_{x_2}\cdot[(\cos(\theta_1)\delta r-(l_0+r)\sin\theta_1\delta\theta_1-l_1\sin\theta_1\delta\theta_1\\ -l_2\sin\theta_2\delta\theta_2]+F_{z_1}\cdot[(\sin(\theta_1)\delta r+(l_0+r)\cos(\theta_1)\delta\theta_1]\\ +F_{z_2}\cdot[(\sin(\theta_1)\delta r+(l_0+r)\cos(\theta_1)\delta\theta_1+l_1\cos\theta_1\delta\theta_1\\ +l_2\cos\theta_2\delta\theta_2].\end{aligned} \tag{32}$$

The external forces included in this LPM are barrier forces, damper forces including front end spring damper system and suspension damper system forces. The corresponding equations are:

$$Q_r^{ext} = Q_r^{bar}+Q_r^{damp}, \tag{33}$$

$$Q_{\theta_1}^{ext} = Q_{\theta_1}^{bar}+Q_{\theta_1}^{damp}, \tag{34}$$

$$Q_{\theta_2}^{ext} = Q_{\theta_2}^{bar}+Q_{\theta_2}^{damp}. \tag{35}$$

Here F_x and F_z are the horizontal and vertical force components acting on the vehicle; Q_r^{bar}, $Q_{\theta_1}^{damp}$ and $Q_{\theta_2}^{damp}$ are the non-conservative barrier and damper forces acting on the system.
Then δU assumes the form

$$\begin{aligned}\delta U = Q_r^{damp}\cdot\delta r+Q_{\theta_1}^{damp}\cdot\delta\theta_1+Q_{\theta_2}^{damp}\cdot\delta\theta_2\\ +Q_r^{bar}\cdot\delta r+Q_{\theta_1}^{bar}\cdot\delta\theta_1+Q_{\theta_2}^{bar}\cdot\delta\theta_2\end{aligned} \tag{36}$$

where

$$\begin{aligned}Q_r^{bar} =& F_{bx_1}\cos\theta_1+F_{bz_1}\sin\theta_1\\ &+F_{bx_2}\cos\theta_1+F_{bz_2}\sin\theta_1,\end{aligned} \tag{37}$$

$$\begin{aligned}Q_{\theta_1}^{bar} =& -F_{bx_1}(l_0+r)\sin\theta_1+F_{bz_1}(l_0+r)\cos\theta_1\\ &-F_{bx_2}[(l_0+r)\sin\theta_1+l_1\sin\theta_1]\\ &+F_{bz_2}[(l_0+r)\cos\theta_1+l_1\cos\theta_1],\end{aligned} \tag{38}$$

$$Q_{\theta_2}^{bar} = -F_{bx_2}l_2\sin\theta_2+F_{bz_2}l_2\cos\theta_2 \tag{39}$$

where F_{bx} and F_{bz} are the barrier forces acting on the vehicle in the horizontal and vertical directions. These values are included from the FE simulation data. The derivative of the dissipation energy D and the damper forces are given by the equations

$$\begin{aligned}D =& \frac{1}{2}c_{comp}\dot{r}^2+\frac{1}{2}c_1[(l_0+r-l_3)\dot{\theta_1}+\dot{r}\theta_1]^2\\ &+\frac{1}{2}c_2[(l_0+r+l_1)\dot{\theta_1}+\dot{r}\theta_1+l_2\theta_2]^2\\ &+\frac{1}{2}c_{tor}\dot{\theta_2},\end{aligned} \tag{40}$$

$$\begin{aligned}Q_r^{damp} =& F_{bx_1}\cos\theta_1+F_{bz_1}\sin\theta_1\\ &+F_{bx_2}\cos\theta_1+F_{bz_2}\sin\theta_1,\end{aligned} \tag{41}$$

$$\begin{aligned}Q_{\theta_1}^{damp} =& -F_{bx_1}(l_0+r)\sin\theta_1+F_{bz_1}(l_0+r)\cos\theta_1\\ &-F_{bx_2}[(l_0+r)\sin\theta_1+l_1\sin\theta_1]\\ &+F_{bz_2}[(l_0+r)\cos\theta_1+l_1\cos\theta_1],\end{aligned} \tag{42}$$

$$Q_{\theta_2}^{damp} = -F_{bx_2}l_2\sin\theta_2+F_{bz_2}l_2\cos\theta_2, \tag{43}$$

where c_1 and c_2 are the damper coefficients for the front and rear suspensions, c_{comp} and c_{tor} are the damper coefficients from the front end compression spring and the torsional spring respectively.

2.3 Validation with an FE Model

The LPM is validated against a modified FEM developed by NHTSA (NHTSA, 2017) where the effect of welding and material behavioural changes in UHSS structural members is included by the authors. The crashworthiness response is affected by the changes in material behaviour which compromise the safety performance. The acceleration, velocity and displacement curves from the 2010 Toyota Yaris FE model for a full frontal impact were used to validate the LPM performance. The speed of the impact was 56 kmph and the barrier is a rigid non deformable barrier with 0% offset. The baseline FE model developed by National Crash Analysis Center (NCAC) and National Highway Transport Safety Administration (NHTSA) (Marzougui et al., 2011), (NHTSA, 2017) was adopted to modify the structural members. The model is cut and welded to incorporate the repairs of UHSS material on load bearing structural members. The material and section properties of the weld were adopted from a similar FE developed in (Noorsumar et al., 2020). The weld zone and HAZ lead to reduced strength in the members and replicates the behaviour in a physical test. It will be interesting to use physical test data in a future study.

Figure 5 shows the FE model developed by NHTSA which replicates a 2010 four-door passenger sedan consisting of 917 parts, 1,480,422 nodes and 1,514,068 elements. The FE model weighs 1,100 kg which is close to the physical test vehicle weighing

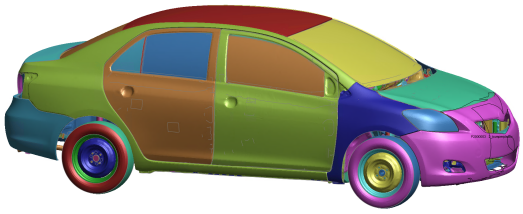

Figure 5: Baseline 2010 Toyota Yaris FE Model.

1,078 kg.The model was correlated with a number of crash loadcases confirming the reliability of the model representing the physical vehicle.

The next section highlights the results and discussion on the model simulations.

3 RESULTS AND DISCUSSION

The LPM defined in the Section 2 was simulated in MATLAB Simulink and the results were compared with the data generated from the LS Dyna FE model for a 2010 Toyota Yaris impacting a rigid barrier at 56 kmph. Prior to overlaying the LS Dyna curve outputs with the LPM results, the FE outputs were converted into polar coordinates to compare the results. The Simulink model was run with an ode45 (variable timestep) solver; it was observed that changing the solver parameters did not influence the results significantly. The maximum values of the pitching angles θ_1 and θ_2 are crucial to determine the occupant injury prediction during the vehicle development stage. The maximum crush of the vehicle and the velocity during energy absorption stage helps predict the vehicle crashworthiness performance in an impact. These parameters have been measured with the Simulink model developed in the study. The values of k_1, k_2, c_1, c_2 have been adopted from (Savaresi et al., 2010) and presented in Table 1.

Table 1: Automotive Parameters set (Savaresi et al., 2010).

Symbol	Value	Unit	Meaning
M	400	kg	Sprung mass
m_{ij}	50	kg	Unsprung masses (i = front, rear and j = left, right)
I_x	250	kg.m^2	Roll inertia
I_y	1400	kg.m^2	Pitch inertia
t	1.4	m	Front and rear axle
l_f	1.4	m	COG-front distance
l_r	1	m	COG-rear distance
r	0.3	m	Nominal wheel radius
h	0.7	m	Chassis COG height
k_f	30,000	N/m	Front suspension linearized stiffness (left, right)
k_r	20,000	N/m	Rear suspension linearized stiffness (left, right)
c_f	1500	N/m/s	Front suspension linearized damping (left, right)
c_r	3000	N/m/s	Rear suspension linearized damping (left, right)
k_t	200,000	N/m	Tire stiffness (front, rear and left, right)
β	50	rad/s	Suspension actuator bandwidth

The front-end spring and damper coefficients (k_{comp} and c_{comp}) were determined from the optimization algorithm presented in Subsection 2.1. The LPM was compared against the data from FE in the parameter identification code. The computed acceleration, velocity and displacement curves are shown in Figure 6. The corresponding spring and damper coefficients are presented in Figure 7.

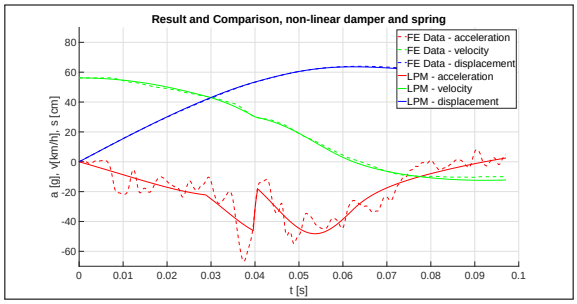

Figure 6: Comparison of FE and LPM curves for parameter identification algorithm.

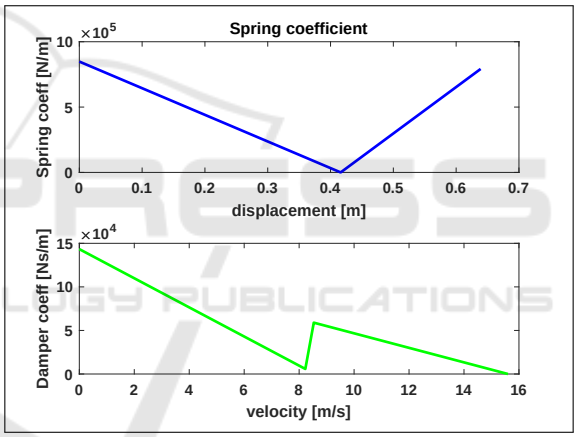

Figure 7: Front-end Spring and Damper coefficients for Toyota Yaris.

The values of m_1, m_2, l_0,l_1, l_2, l_3, k_{tor}, c_{tor} along with external forces F_{bx_1}, F_{bz_1}, F_{bx_2}, F_{bz_2} were calculated from the LS Dyna model and presented in Table 2.

Table 2: Model Parameters.

Mass Body 1 m_1	539 kg
Mass Body 2 m_1	629 kg
l_1	0.57 (metres)
l_2	1.3 (metres)
l_3	0.10 (metres)
l_0	0.91 (metres)
k_{tors}	Curves from LS Dyna model
c_{tors}	Curves from LS Dyna model

Figure 8 shows the change in the velocity of the vehicle in m/s after the impact. The LPM was over-

laid with the FE data curves and the plots show good correlation of the time when the vehicle attains zero velocity. The trend of the curves is similar indicating the impact kinematics has been replicated in the LPM. The maximum deformation experienced by the vehicle during the full frontal impact is shown in Figure 9 and the maximum crush values are closely correlated, demonstrating a good prediction capability of the model.

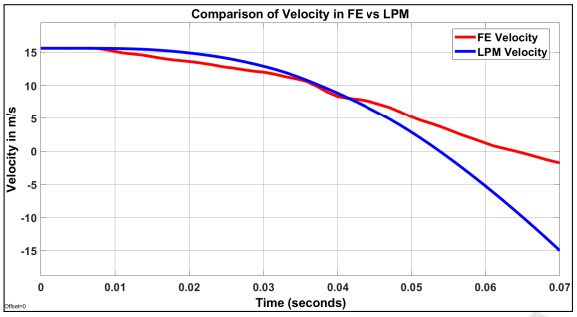

Figure 8: Velocity of the vehicle - curves comparison for LPM vs FE model.

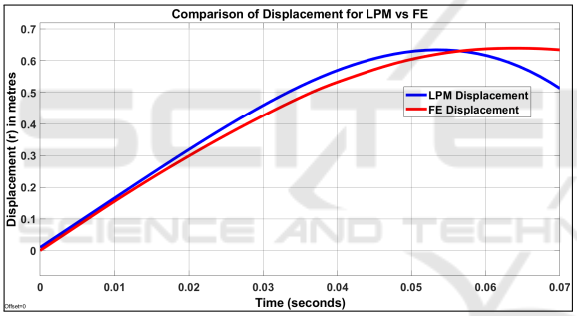

Figure 9: Displacement of the vehicle front-end - curves comparison for LPM vs FE model.

Figure 10 shows the plot of θ_1 which indicates the pitching of the vehicle about the point of impact. The curves for the LPM over-predict the maximum pitching angle; this could be attributed to the approximation of the model parameters like suspension spring and damper coefficients which were assumed to be constant throughout the simulation. It is however, crucial to predict the maximum pitching angle to design the restraint systems for occupants in the vehicle; the pitching angle θ_1 is closely correlated in the LPM developed in this study.

As explained in Section 2, the model uses a torsional spring to represent fractures in the structural members due to HAZ (from welding or heat treatment processes); leading to an angle θ_2 in the vehicle pitching. The plot for θ_2 is shown in Figure 11; the stiffness of the spring is approximated from the weld failure data used in the FE model. It is observed that the predicted angle from the LPM is close to the maximum value from the FE model, however, the model can be further improved.

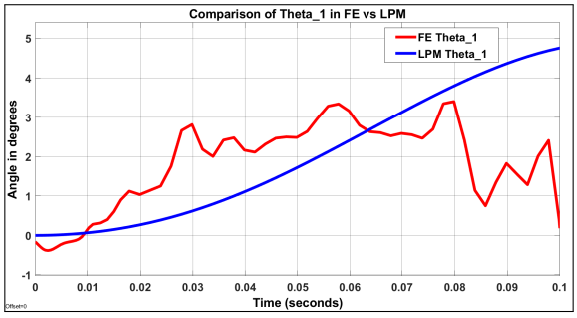

Figure 10: θ_1 curve comparison for LPM vs FE model.

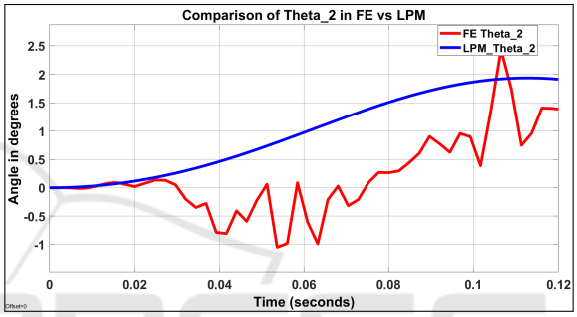

Figure 11: θ_2 curve comparison for LPM vs FE model.

4 CONCLUSIONS AND NEXT STEPS

The reliability of mathematical modeling to replicate and predict vehicle crashworthiness response has increased during the last decade. These models are slowly replacing physical tests; LPMs provide results with low computational time and fewer vehicle parameters. LPMs can be used during the initial stages of the vehicle development process when full scale CAD models are not available. The literature review indicated little research in the area of representing welds and material failure in LPMs. Our 3 DOF LPM predicts the following vehicle parameters in a full frontal impact:

- Maximum vehicle crush during an impact.
- Time for the vehicle to reach zero velocity from the start of the event.
- Vehicle pitching angle about the point of impact.
- Failure of the structural members leading to higher pitching angle in a modified vehicle.

The model uses an elastic double compound pendulum replicating the event kinematics to capture the

front-end deformation and the rotation of the vehicle; first around the point of impact and then around the failure of the material due to welding or heat treatment. The LPM employs Lagrangian formulation to define the equations of motion and is presented in polar coordinates to simplify the system. The model correlates well with the FE data for a 2010 Toyota Yaris; the deformation, velocity and pitching angle are predicted well for a full frontal impact at 56 kmph. The failure of the structural members is simulated in the model with a torsional spring. The angle of rotation of the vehicle θ_2 due to material behavioural changes is close to the maximum values in the validation data.

The novel methodology presented in this study can be further enhanced with real-time weld fracture data from physical tests. The model predictability can be further improved by replacing the piece-wise linear approximation for the vehicle parameter values with non-linear functions for stiffness and damping coefficients.

ACKNOWLEDGEMENTS

The authors would like to thank Top Research Center Mechatronics (TRCM) at University of Agder for the support to conduct the research. We would also like to acknowledge the support of NHTSA and NCAC for the FE models used in this study.

REFERENCES

Amirthalingam, M., Hermans, M., and Richardson, I. (2009). Microstructural development during welding of siliconand aluminum-based transformation-induced plasticity steels-inclusion and elemental partitioning analysis. *Metallurgical and Materials Transactions A: Physical Metallurgy and Materials Science*, 40(4):901–909.

Benson, D., Hallquist, J., Igarashi, M., Shimomaki, K., and Mizuno, M. (1986). Application of DYNA3D in large scale crashworthiness calculations.

Böttcher, C. S., Frik, S., and Gosolits, B. (2005). 20 years of crash simulation at Opel-experiences for future challenges. *4th LS-DYNA Anwenderforum*, pages 79–86.

Chang, J. M., Ali, M., Craig, R., Tyan, T., El-Bkaily, M., and Cheng, J. (2006a). Important modeling practices in CAE simulation for vehicle pitch and drop. In *SAE Technical Papers*. SAE International.

Chang, J. M., Huang, M., Tyan, T., Li, G., and Gu, L. (2006b). Structural optimization for vehicle pitch and drop. In *SAE Technical Papers*. SAE International.

Cyrén, O. and Johansson, S. (2018). Modeling of Occupant Kinematic Response in Pre-crash Maneuvers A simplified human 3D-model for simulation of occupant kinematics in maneuvers.

Elkady, M. and Elmarakbi, A. (2012). Modelling and analysis of vehicle crash system integrated with different VDCS under high speed impacts. *Central European Journal of Engineering*, 2(4):585–602.

Elkady, M., Elmarakbi, A., and Macintyre, J. (2012). Enhancement of vehicle safety and improving vehicle yaw behaviour due to offset collision using vehicle dynamics. *International Journal of Vehicle Safety*, 6(2):110–133.

Goldstein, H., Poole, C., Safko, J., and Addison, S. R. (2002). Classical Mechanics, 3rd ed. *American Journal of Physics*, 70(7):782–783.

Ionut, R. A., Corneliu, C., and Bogdan, T. (2017). Mathematical model validated by a crash test for studying the occupant's kinematics and dynamics in a cars' frontal collision. *International Journal of Automotive Technology 2017 18:6*, 18(6):1017–1025.

Kamal, M. M. (1970). Analysis and simulation of vehicle to barrier impact. *SAE Technical Papers*, pages 1498–1503.

Marzougui, D., Brown, D., Park, H. K., Kan, C. D., and Opiela, K. S. (2011). 3 th International LS-DYNA Users Conference Session: Automotive Development & Validation of a Finite Element Model for a Mid-Sized Passenger Sedan.

Mentzer, S. G., Radwan, R. A., and Hollowell, W. T. (1992). The SISAME methodology for extraction of optimal lumped parameter structural crash models. *SAE Technical Papers*.

NHTSA (2017). Crash simulation vehicle models.

Noorsumar, G., Robbersmyr, K., Rogovchenko, S., and Vysochinskiy, D. (2020). Crash Response of a Repaired Vehicle - Influence of Welding UHSS Members. In *WCX SAE World Congress Experience*. SAE International.

Noorsumar, G., Rogovchenko, S., Robbersmyr, K., and Vysochinskiy, D. (2021a). Mathematical models for assessment of vehicle crashworthiness: a review. *International Journal of Crashworthiness*.

Noorsumar, G., Rogovchenko, S., Robbersmyr, K., Vysochinskiy, D., and Klausen, A. (2021b). A novel technique for modeling vehicle crash using lumped parameter models. In *Proceedings of the 11th International Conference on Simulation and Modeling Methodologies, Technologies and Applications, SIMULTECH 2021*.

Noorsumar, G., Vysochinskiy, D., Englund, E., Robbersmyr, K. G., and Rogovchenko, S. (2021c). Effect of welding and heat treatment on the properties of UHSS used in automotive industry. *EPJ Web of Conferences*, 250:05015.

Pavlov, N. (2019). Study the vehicle pitch motion by spring inverted pendulum model. (February).

Pifko, A. and Winter, R. (1981). *Theory and Application of Finite Element Analysis To Structural Crash Simulation*, volume 13. Pergamon Press Ltd.

Savaresi, S., Poussot-Vassal, C., Spelta, C., Sename, O., and

Dugard, L. (2010). *Semi-Active Suspension Control Design for Vehicles*. Elsevier Ltd.

Subedi, D., Tyapin, I., and Hovland, G. (2020). Modeling and Analysis of Flexible Bodies Using Lumped Parameter Method. In *Proceedings of 2020 IEEE 11th International Conference on Mechanical and Intelligent Manufacturing Technologies, ICMIMT 2020*, pages 161–166. Institute of Electrical and Electronics Engineers Inc.

Sypniewska-Kamińska, G., Starosta, R., and Awrejcewicz, J. (2016). Double pendulum colliding with a rough obstacle. In *Dynamical Systems - Mechatronics and Life Sciences*. Instytut Mechaniki Stosowanej, Wydział Budowy Maszyn i Zarządzania, Politechnika Poznańska.

Sypniewska-Kamińska, G., Starosta, R., and Awrejcewicz, J. (2017). Motion of double pendulum colliding with an obstacle of rough surface. *Arch Appl Mech*, 87:841–852.

Zhang, M., Li, L., Fu, R. y., Zhang, J. c., and Wan, Z. (2008). Weldability of Low Carbon Transformation Induced Plasticity Steel. *Journal of Iron and Steel Research, International*, 15(5):61–87.